Evidence for a correlated electron state from shot noise in bad-metal nanojunctions

Yiou Zhang,[1,*] Chendi Xie,[2,†] John Bacsa,[2] Yao Wang,[2] and Sergei Urazhdin[1]
[1]*Department of Physics, Emory University, Atlanta, Georgia 30322, USA*
[2]*Department of Chemistry, Emory University, Atlanta, Georgia 30322, USA*

(Received 4 October 2025; revised 3 February 2026; accepted 12 February 2026; published 2 March 2026)

We report anomalously large shot noise in metallic and tunnel nanojunctions of β-tantalum, a metal characterized by a small negative temperature coefficient of resistivity inconsistent with both the Fermi liquid theory of Bloch electrons and single-particle localization. Fano factors are enhanced, and cluster around even multiples of the values expected for Fermi liquids, suggesting the possibility of pairwise electron correlations akin to local groups of Cooper pairs. The importance of spin for this state is suggested by the effects of magnetic impurities. Additional evidence for correlations is provided by the reduced density of states near the Fermi level revealed by point contact spectroscopy and first principles calculations. Our findings indicate that electron correlations may play an important role in a much larger class of materials than previously believed.

DOI: 10.1103/spvt-n2hz

I. INTRODUCTION

Exotic electronic states not described by the single-particle Fermi liquid (FL) picture can emerge close to quantum critical points such as the metal-insulator transition [1]. Based on the Ioffe-Regel criterion, electron localization is expected if the material resistivity ρ exceeds a crossover value corresponding to a mean free path shorter than the lattice constant, about 1.5 $\mu\Omega$ m in common transition metal alloys [2]. However, a wide range of materials called "bad" metals remain metallic in the Ioffe-Regel limit. Bad metals often exhibit a small nondivergent negative temperature coefficient of resistivity (TCR), described as "weak" or "failed" insulators [3,4]. These behaviors are inconsistent with both single-electron localization and diffusive transport.

Among bad metals are unconventional superconductors [5–7] and other strongly correlated materials [8–12], suggesting that bad metallicity may involve many-particle effects [3,13,14]. A large magnetoresistance observed in some conventional superconducting (SC) bad metal films close to the critical temperature T_C [15–18] was attributed to the correlated state termed the Bose liquid [3,13,19–23]. This state was hypothesized to host incoherent Cooper pairs [4] or a local pair condensate that lacks long-range phase coherence [24]. However, there is presently no direct evidence for the Bose liquid state in bad metals that are either non-SC or at temperatures far above their T_C. Since bad metallicity often persists at room temperature, the existence of such a state may imply pairing mechanisms potentially relevant to high-temperature superconductivity.

The β allotrope of tantalum (Ta) is an archetypal elemental bad metal and a failed insulator [see Fig. 1(b)], which is widely used in spin orbitronics as a spin current source due to its large spin Hall effect (SHE) [25]. The α allotrope of Ta, a typical FL, exhibits a significantly smaller SHE, suggesting that the mechanism responsible for bad metallicity may be also important for spin Hall efficiency. Motivated by the observation that bad metallicity of β-Ta cannot be explained by single-particle disorder, Refs. [26,27] studied electron-electron (e-e) interaction effects by utilizing shot noise (SN) measurements in β-Ta nanowires and metallic junctions (MJs). SN is white noise caused by the discrete nature of charge carriers. For tunnel junctions (TJs), its current spectral density is $S_I = 2FeI$, where I is current, $F = q/e$ is the Fano factor, q is the charge of elementary excitations and e is the electron charge, and thermal effects are neglected [28]. Since the Fano factor is dependent on the charge of elementary excitations, SN provides a sensitive measure of electron correlations. In particular, Fano factor doubling was demonstrated in TJs based on superconductors due to Cooper pairing [29,30].

The properties of SN in non-SC TJs are expected to be independent of the tunnel barrier height and width as long as the transmission probabilities through all the conduction channels are substantially smaller than 1. In contrast, MJs are characterized by the dominant transmission through almost open conduction channels, resulting in Ohmic transport. In this case, the SN properties are determined by the transport regime and electron-phonon interactions. Diffusive transport of charges q in a short MJ is expected to give $F = q/3e$, while thermalization due to e-e interaction is expected to result in the "hot" electron regime where $F = \sqrt{3}/4$ is determined by the fluctuation-dissipation relation [31]. SN suppression in "strange" metal nanowires was attributed to a correlated electron liquid that lacks single-electron excitations [32,33]. Similar behaviors were observed in β-Ta nanowires [26], but were subsequently shown to result from electron-phonon interactions [27]. Measurements of nanometer-scale β-Ta junctions revealed the hot electron regime in junctions as short

*Contact author: yiou.zhang@emory.edu
†Also at Department of Physics and Astronomy, Clemson University, Clemson, SC 29631, USA.

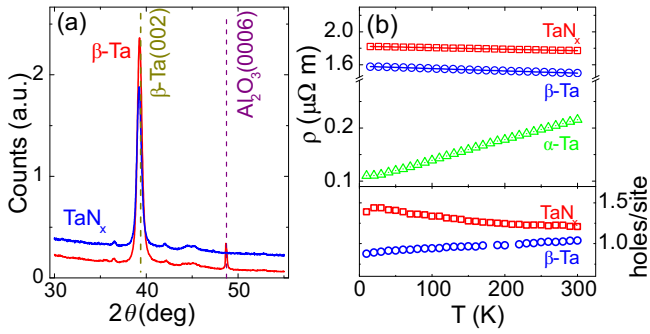

FIG. 1. (a) XRD $\theta - 2\theta$ scan on β-Ta(35) and TaN_x(35) on Al_2O_3 (0001) using the Co K_α line. Tilting by $\approx 2^\circ$ off-Bragg was used to minimize substrate reflections. The curves are offset for clarity. The expected positions $2\theta = 39.36^\circ$ and 48.84° of the β-Ta(002) and Al_2O_3(0006) peaks are indicated. (b) Resistivity (top) and carrier concentration from the Hall data (bottom) for 15-nm-thick β-Ta, TaN_x, and α-Ta films, as labeled. Solid lines are fittings based on the electron interaction-mediated hopping model [27], giving electron interaction-mediated conductivities of 0.63 and 0.51 MS/m for β-Ta and TaN_x, respectively.

as 8 nm, suggesting strong e-e interactions [27]. However, the nature of many-electron states resulting from these strong interactions remains unknown. Notably, the superconducting transition temperature $T_C < 1$ K in β-Ta [34] is far below the temperature range where bad metallicity and anomalous SN are observed. Thus, the underlying correlations are likely distinct from the conventional superconducting pairing, and may instead involve the Mott-Hubbard mechanism as discussed in the Supplemental Material (SM) [35].

Here, we present evidence suggesting a correlated state in β-Ta, by utilizing SN measurements in TJs and point-contact (PC) MJs. The effective length of PC MJs is significantly shorter than in the previously studied MJs, minimizing the electron thermalization effects that prevented characterization of carrier charge. Our results advance SN measurements as an efficient approach to studies of e-e interactions, and provide insight into the correlations underlying anomalous metallic states.

II. METHODS

The studied junctions were formed by Ta layers sandwiched between two current-carrying metallic Au electrodes [see inset in Fig. 2(a)]. It is established that pure β-Ta can

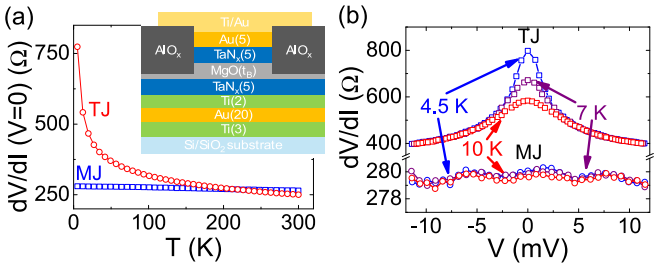

FIG. 2. R vs T (a) and V (b) for a TJ and MJ, as labeled. The inset in (a) is the cross-section schematic of the junctions.

be obtained by deposition directly on a sapphire substrate after a short Ar ion bombardment to activate its surface polar bonds [26]. We used this method to deposit the reference β-Ta films discussed below. In contrast, pure Ta grown on metallic buffer layers forms the α allotrope [26,27]. To overcome this issue, we developed a method to obtain a well-defined β allotrope of Ta deposited on metallic layers. This was accomplished by sputtering 99.9% pure Ta in the presence of a small partial pressure $P_N = 4 \times 10^{-6}$ Torr of ultrapure nitrogen, in addition to the ultrahigh purity Ar processing gas at $P_{Ar} = 4 \times 10^{-3}$ Torr, in an ultrahigh-vacuum chamber with the base pressure of 4×10^{-9} Torr.

X-ray diffraction (XRD) for the test films deposited on a Ti(1) buffer layer (the number is thickness in nanometers) showed a single β-Ta (002) peak slightly shifted and reduced in amplitude compared to pure β-Ta, with no signatures of impurity or α phases [Fig. 1(a)]. Energy dispersive spectroscopy showed that a small amount of nitrogen became incorporated in the film, forming a nominal composition TaN_x with $x = 9 \pm 2\%$ (see SM [35]). However, the lack of noticeable XRD peak broadening shows that nitrogen was predominantly incorporated into the grain boundaries and/or as interstitial, without significantly changing the β-Ta structure. This is consistent with the slight shift of the XRD peak corresponding to the tensile lattice strain of $\approx 0.3\%$.

Hall measurements gave carrier concentration of one hole per atom in β-Ta, and a slightly higher hole concentration in TaN_x, as expected from nitrogen doping. The Hall carrier concentrations show a small temperature dependence with opposite trends. To the best of our knowledge, there is no established general theory of the Hall effect in non-FLs, warranting further analysis of the mechanisms underpinning these differences. The mean free path is somewhat reduced by nitrogen incorporation (see SM [35]). The resistivity is slightly increased but its temperature dependence remains nearly the same as in pure β-Ta [Fig. 1(b)]. Both dependences can be fitted using the electron interaction-assisted hopping model of Ref. [27] [solid lines in Fig. 1(b)] with the contribution of e-e interaction to hopping decreased due to nitrogen doping by about 25%. Based on these results, we conclude that the effects of e-e interaction in TaN_x described below are also relevant to and likely more significant in pure β-Ta.

The studied junctions were based on multilayers formed by two TaN_x electrodes separated by an MgO tunnel barrier and sandwiched between conducting Au electrodes [inset in Fig. 2(a)]. We have also fabricated junctions based on the AlO_x tunnel barrier. They showed a very large flicker noise (FN) likely caused by the charge trapping in defects at the AlO_x/Ta interface, which prevented SN characterization in these junctions.

All the materials are dc sputtered except for MgO, which is rf sputtered. The multilayer films were vacuum annealed at 300 °C for 2 h and patterned into micron-scale junctions by electron-beam lithography. MgO barrier thickness $t_B = 2.9$ nm for TJs was chosen so that the junction resistance was in the range $R = 0.2$–2 kΩ, which optimizes the sensitivity of our noise measurement setup.

According to the theories of tunneling between metallic electrodes through an insulating barrier, the TJ resistance is expected to decrease with increasing bias V and increasing

temperature T [37,38]. In contrast, transport through a pinhole in a TJ is Ohmic, i.e., its resistance R is independent of V and T. Thus, the bias and the temperature dependence provide two distinct criteria for the characterization of junction quality, as illustrated in Fig. 2 for a representative TJ. We did not observe any noticeable variations in the electronic properties of the studied junctions as a function of time or bias history, allowing us to conclude that memristive effects associated with oxygen migration in the MgO barrier or nitrogen migration in TaN_x were negligible. We attribute this stability to negligible thermal activation at cryogenic temperatures where noise measurements were performed.

To independently confirm that the anomalous SN is not associated with specific junction chemistry, we also studied nanoscale MJs. The latter were naturally formed in some samples due to pinholes in the tunnel barrier, as was evidenced by the bias- and temperature-independent junction resistance distinct from the dependences observed for TJs. The naturally formed junctions were not sufficiently stable for SN measurements. Instead, the studied MJs were formed by applying voltage pulses until junction resistance dropped to $R \approx 300\ \Omega$. Since the insulating barrier is known to break down in "hot spots" with the smallest local barrier thickness, such junctions form small pinholes the resistance of which can be comparable to TJs. Since our noise measurement setup is designed for junction resistance $R = 0.2$–$2\ \mathrm{k}\Omega$, we further optimized measurement sensitivity by using a slightly thicker 3.5-nm MgO layer in these junctions. Before the voltage bias-induced breakdown, their resistance was in the few-kΩ range. Thus, shunting of the pinhole by conduction through the insulating layer was minimized. Because of the dominance of hot spots, the effective length of the junctions formed using this approach is likely significantly smaller than the nominal barrier thickness $t_B = 3.5$ nm, avoiding electron-phonon scattering effects that can compromise SN measurements in nanowires [26]. After the junction was formed, no further variations of the junction resistance were observed when additional voltage pulses of either polarity were applied. Thus, the possibility of memristivelike history dependence of junction properties [39], including the noise discussed below, can be ruled out.

We emphasize that the junction resistance by itself does not allow one to distinguish TJs from MJs since it is dependent on the effective junction area, which can be much smaller for the MJs due to their pinhole conduction mechanism. For $R \approx 300\ \Omega$, we estimate the effective junction size of 2–3 nm. We confirmed the metallic conduction in our MJs by the lack of resistance dependence on T or V (Fig. 2). This eliminates the possibility of memristive behaviors in transport properties of noise produced by the junctions, since bias history dependence necessarily requires bias dependence.

To characterize the SN, voltage noise $S_V = (dV/dI)^2 S_I$ was measured by the cross-correlation technique, as reported elsewhere [33] (see also SM [35]). The noise spectra were analyzed to elucidate the contribution from the FN, which was identified by the $1/f$ spectrum, a quadratic increase with bias, and an increase with T [40]. Each data point was obtained by averaging multiple crosscorrelated spectra in the noise frequency window determined by two conditions. First, the noise did not exhibit electromagnetic interference, which is manifested by sharp bias-independent peaks. Second, the frequency-dependent flicker noise could be accurately fitted and its contribution subtracted from the measured noise (see SM [35]). We note that this approach was used to extend the SN measurement bias range. At small bias, the flicker noise contribution was negligible. The acquisition time was 30–300 s per point depending on the frequency window. The calibration and measurement approaches were verified using $Al/AlO_x/Al$ TJs, yielding Fano factor $F = 1$ as expected for single-electron tunneling between Al electrodes [35].

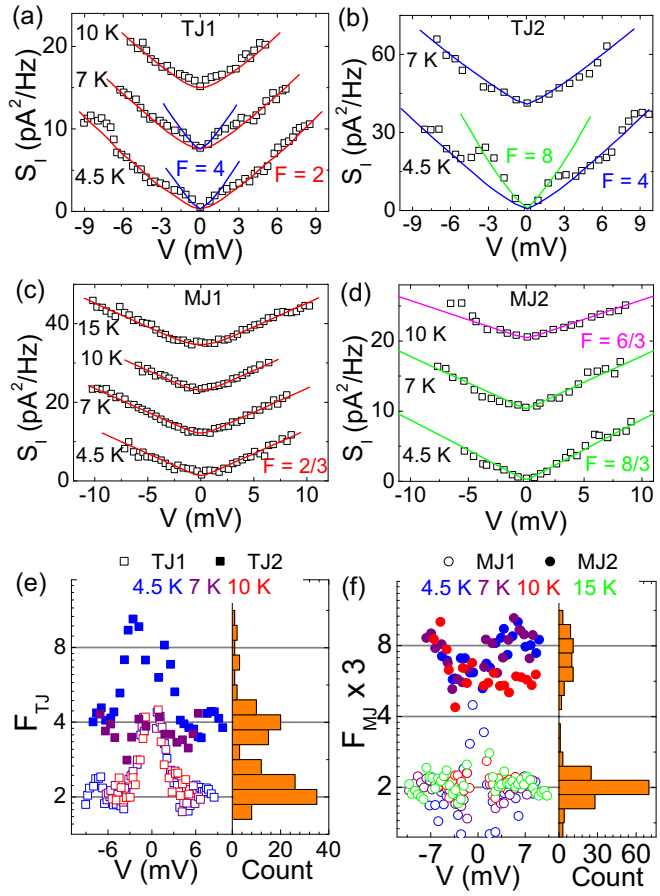

FIG. 3. (a)–(d) Shot noise vs bias for two TJs (a), (b) and MJs (c), (d), at the labeled T. The noise data for different temperatures are offset for clarity. The curves are fittings with Eq. (1) for TJs and Eq. (2) for MJs. (e), (f) F vs bias for TJs (e) and MJs (f), and histograms of the corresponding distributions.

III. RESULTS

Figures 3(a)–3(d) show $S_I(V)$ for two TJs and two MJs. Nine additional TJs and seven MJs show similar behaviors in the range of T and V limited by the onset of FN [35]. For all the junctions, the noise increases approximately linearly with bias above a few mV, consistent with the expectations for SN.

We used two complementary approaches to extract information about the charge carriers from these measurements. In the first approach, the dependence of noise on bias was fitted using a generalization of the dependences expected for

the FLs. The noise produced by a FL TJ is [28,33]

$$S_I(V) = \frac{2eV}{R} \coth \frac{eV}{2k_BT},$$

where $R = dV/dI$ is the differential resistance and k_B is the Boltzmann constant. The corresponding Fano factor is $F = 1$. The noise power produced by tunneling of charges $q = F_{\rm TJ}e$ is then

$$S_I(V) = \frac{2F_{\rm TJ}eV}{R} \coth \frac{F_{\rm TJ}eV}{2k_BT}. \quad (1)$$

For single-electron diffusion in a FL MJ, both the random matrix approximation [41] and semiclassical Boltzmann equation [42,43] predict

$$S_I(V) = \frac{2eV}{3R} \coth \frac{eV}{2k_BT} + \frac{8}{3}\frac{k_BT}{R},$$

which gives the Fano factor $F = 1/3$. An extension of this equation obtained by replacing e with $F_{\rm MJ}e$ is

$$S_I(V) = \frac{2F_{\rm MJ}eV}{3R} \coth \frac{F_{\rm MJ}eV}{2k_BT} + \frac{8}{3}\frac{k_BT}{R}. \quad (2)$$

These equations describe a crossover between a linear dependence dominated by SN at $V >\!\!> k_BT$ with the slope given by the Fano factor, and the thermal regime dominated by Johnson noise $S_v = 4k_BTR$ at $V \gg k_BT$. An empirical form slightly different from Eq. (2) was proposed in Ref. [32] for MJs, resulting in minor differences between the expected thermal broadening not essential for the analysis below.

The Fano factors extracted from the fittings for all the studied TJs and MJs with Eqs. (1) and (2), respectively, are anomalously large, and cluster around even multiples (2, 4, 6, and 8) of the values expected for FLs [Figs. 3(a)–3(d) and SM [35]]. We do not observe any noticeable correlation between junction resistance and variations in F among different junctions. The Fano factors in the TJs are enhanced at small V, which is reminiscent of the increase due to Cooper pairing in SC TJs at bias below the SC gap [30,44]. The steplike noise variation associated with the enhancement does not correspond to any features in the differential conductance (see Fig. 2), ruling out bias-dependent conduction channel opening as a possible mechanism.

The uncertainties in our fitting of the limited dataset leave room to alternative interpretations of Fano factor enhancement at small bias. Nevertheless, these features are symmetric with respect to the bias polarity, confirming that they are not random noise variations. We also note that the possible artifacts due to FN are minimized at small bias, and cannot account for the observed Fano factor enhancement.

Importantly, the enhanced Fano factors are almost temperature independent in MJs. For TJs, they show a decrease at small bias but remain enhanced. These observations indicate that the correlations that underpin the enhanced SN originate from a robust interaction mechanism not directly related to superconducting ordering observed in β-Ta only below 1 K [45].

To further test our observation that F may cluster around even multiples of values expected for FLs, we used an alternative approach to data analysis based on the observation that the magnitude of noise at a single bias point $V \gg k_BT$ can characterize the carrier charge. We define the Fano factor for individual data points as $F_{\rm TJ} = S_IR/2eV$ for TJs, and $F_{\rm MJ} = (S_IR - 8k_BT/3)/2eV$ for MJs. The former expression neglects thermal effects the relative contribution of which is larger in MJs due to smaller F, and is accounted for in the latter expression. The calculated distribution of F is quasicontinuous due to transitions between different regimes and thermal broadening at small V. Nevertheless, both $F_{\rm TJ}$ and $3F_{\rm MJ}$ cluster around even values, Figs. 3(e) and 3(f). We note that this result may be influenced by artifacts due to uncertainties stemming from the limited noise statistics and a possible non-negligible contribution from FN. Point-to point variation in Figs. 3(a)–3(d) provides an estimate of random noise comparable to the symbol size. However, the potential systematic uncertainty from FN is more difficult to estimate.

We emphasize that the apparent clustering of Fano factors around even values is suggestive but not conclusive, due to the limitations of data statistics and of the interpretation of Fano factor values based on individual noise data points. These limitations warrant additional studies of shot noise in junctions based on other correlated metals and different barriers. Junctions of van der Waals (VdW) materials are particularly attractive thanks to the ability to judiciously engineer pinhole-free ultrathin barriers with atomic precision. This approach requires highly transparent VdW junction contacts to minimize the contact contribution to noise [46]. The reduced charge trapping in atomically thin barriers can result in smaller flicker noise, facilitating measurements over a larger bias range and enabling precise Fano factor determination.

The results of noise measurements indicate that charge current in the studied TJs and MJs may be carried by electron groups rather than single electrons, suggesting a correlated electron state. We now present additional theoretical and experimental evidence supporting this possibility. Because of the lattice complexity and multiorbital electronic structure of β-Ta, many-body simulations that could verify whether anomalous SN in β-Ta may be caused by correlations are impractical. Instead, we performed comparative first principles band structure calculations based on two different approximations for the exchange-correlation functional: the Perdew-Burke-Ernzerhof (PBE) and r^2 strongly constrained and appropriately normed (r^{2}SCAN) metageneralized gradient approximation (mGGA) [47]. Neither the PBE nor the r^{2}SCAN approximations capture many-particle effects [48], but the latter better accounts for correlations [47,49]. Thus, their differences can provide insight into correlations even in single-particle approximation.

The calculations utilized the QUANTUM ESPRESSO package [50], which is based on the plane-wave pseudopotential method. The PBE calculations were based on the exchange-correlation functional with SG-15 optimized norm-conserving Vanderbilt pseudopotentials [51,52]. Structural relaxation was performed using the r^{2}SCAN [47] functional with a semiempirical Grimme DFT-D2 van der Waals correction [53]. The r^{2}SCAN electronic structure calculations were performed using the same r^{2}SCAN functional with the relaxed structures. A cutoff energy of 200 Ry was used to expand the wave functions, and a Γ-centered Monkhorst-Pack sampling [54] of $4 \times 4 \times 8$ was adopted for the integral over the Brillouin zone.

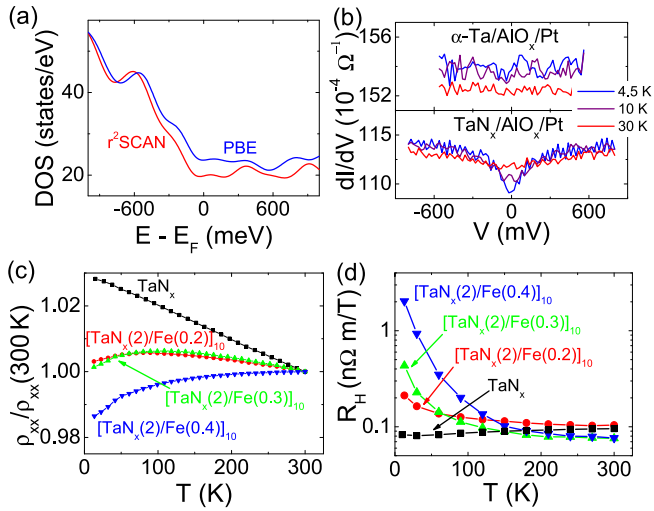

FIG. 4. (a) DOS of β-Ta calculated using the r^{2}SCAN mGGA and PBE functionals. (b) Conductance spectra of TaN_x and α-Ta PCs. (c) Resistivity and (d) Hall coefficient of Ta/Fe multilayers vs T.

The convergence criterion of the corresponding electronic self-consistent field was set to 10^{-10} Ry.

The density of states (DOS) calculated using r^{2}SCAN is reduced near the Fermi energy compared to the PBE functional, Fig. 4(a). Comparing the calculated band structures (see SM [35]), this is associated with the overall shift of the bands away from the Fermi surface, consistent with the effects of correlations. We emphasize that the band picture is inconsistent with the failed insulator properties of β-Ta, so these calculations provide only single-particle signatures of the many-electron correlation effects, and are not capable of capturing their magnitude.

To investigate the possibility of DOS suppression in β-Ta, we performed additional PC spectroscopy. The PCs were fabricated from multilayers similar to those in SN measurements, except the MgO barrier was replaced by sputtered AlO_x (t_B = 3.5 nm) and annealing was not performed, resulting in metallic PCs through pinholes in AlO_x. Additionally, the TaN_x layer on top of AlO_x was replaced by Pt, so that the PC spectra were determined entirely by the electronic structure of the bottom electrode, either TaN_x or α-Ta. The latter was grown by sputtering Ta in pure Ar, as discussed above.

The differential conductance of a PC based on α-Ta is independent of bias, as expected for weakly energy-dependent DOS in the FL [Fig. 4(b)]. In contrast, the conductance of PC based on β-Ta decreases at small bias, which becomes more pronounced at lower T. The variation occurs on a significantly larger bias scale than in MgO [Fig. 2(b)] and $Al/AlO_x/Al$ TJs (see SM [35]), and conductance is significantly higher than in TJs. This cannot be explained by tunneling effects but is consistent with reduced DOS near the Fermi level. The symmetric PC spectra do not reflect the asymmetry of the calculated band structure [Fig. 4(a)], confirming that the single-electron band approximation is inadequate. The symmetric bias dependence also indicates that the junction resistance is not influenced by the Schottky effect.

If electron correlations are spin dependent, they are expected to be suppressed by magnetic field. In the qualitative picture discussed below, these correlations involve electrons quasilocalized on the neighboring sites. The required fields are then of the order $B \sim \Phi_0/d^2 \approx 10^4$ T, too large for direct testing of field effects. Here, Φ_0 is the flux quantum and $d = 0.28$ nm is interatomic spacing. On the other hand, effective exchange fields in magnetic materials are of the same order of magnitude. To test their effects on β-Ta, we introduced a proximity-induced effective exchange field via magnetic impurities, in multilayers with the structure $[TaN_x(2)Fe(t_{Fe})]_{10}AlO_x(3)$ where t_{Fe} ranged between 0.2 and 0.4 nm. The films were annealed in vacuum at 300 °C for 2 h to promote the formation of magnetic nanoclusters. In contrast to TaN_x, these films exhibit a positive TCR at cryogenic T, with the crossover temperature to negative TCR that increases with t_{Fe} [Fig. 4(c)]. This cannot be explained by the parallel conductance though Fe, in which case the opposite temperature dependence would be observed due to the saturation of Fe resistivity at cryogenic T. The onset of positive TCR coincides with the enhancement of the Hall coefficient [Fig. 4(d)], as expected from the anomalous Hall contribution due to the onset of magnetism in Fe clusters. We conclude that bad metallicity is suppressed by magnetism, supporting its origin from Mott singletlike correlations. The large magnitude of the effective exchange field needed to suppress this state confirms that the correlations are short ranged.

IV. DISCUSSION

Our central result is the observation of enhanced SN in TaN_x nanojunctions, suggesting a correlated state. First, we discuss potential alternatives. Enhanced noise cannot be an artifact due to FN, as we do not observe any correlation between F and FN among different samples, and the largest enhancement of F in TJs is at small bias where FN is negligible. Cooper pair tunneling in SC junctions results in doubled F, and Andreev reflections due to SC gap can further enhance SN [55]. However, this mechanism is not relevant to gapless non-SC β-Ta.

SN enhancement in TJs can be caused by intermittent blocking of tunneling through a localized state in the barrier, due to interaction with another localized state [56–58]. However, analysis shows that this mechanism generally results in asymmetric dependence on bias direction, and even in special cases where it is symmetric F should continuously evolve with bias, inconsistent with our results (see SM [35] for details).

We now propose a microscopic model for our observations. We emphasize that our model is qualitative; many-electron theoretical analysis and simulations are necessary for its validation. Each atom in β-Ta is coordinated by 20 nearest or next-nearest neighbors within a narrow distance range $d = 0.28$–0.284 nm [59,60], resulting in a low-symmetry but almost isotropic crystal field. Large spin-orbit coupling (SOC) splits the $5d$ levels into the $J = 5/2$ sextuplet and $J = 3/2$ quadruplet. The latter is occupied by the three valence electrons, consistent with the measured charge density of one hole per atom.

To analyze the electronic properties of β-Ta, we calculate the Koster-Slater amplitudes for hopping among the $J = 3/2$

states. These amplitudes are determined by two matrix elements, $V_1 = V_{dd\sigma} + V_{dd\pi} - 2V_{dd\delta}$ and $V_2 = 2(V_{dd\pi} + 4V_{dd\delta})$, where $V_{dd\sigma} = 6V_{dd\delta} = -3V_{dd\pi}/2$ in the atomic sphere approximation [61,62] (see SM [35] and Ref. [63]). Both V_1 and V_2 vanish, so only hybridization beyond this approximation contributes to hopping. Hopping suppression is evident from the small bandwidths $2t \lesssim 0.5$ eV in the first principles calculations (see SM [35]), significantly smaller than the Mott-Hund energy $U = 2$–3 eV [64].

In single-orbital systems, the condition $t \ll U$ implies that charges become localized at half filling, or form a strongly correlated state at sufficient deviations from half filling. The effects of large interaction in multiorbital systems are less explored [65]. Our Mott-Hubbard analysis shows that in this case, dephasing of the single-particle wave function due to electron interactions also leads to localization, which for multiorbital systems does not result in MIT due to the absence of Pauli blocking (see SM [35] for details). The temperature-dependent resistivity of β-Ta and TaN_x can be accurately fitted by the parallel-resistor formula [2] based on a combination of the usual Mott phonon-mediated quasilocalized charge hopping and e-e interaction-assisted hopping, as shown by solid lines in Fig. 1(b). The phonon contribution to hopping decreases with decreasing T while the e-e assisted contribution is temperature independent, resulting in a large overall resistivity and small nondivergent negative TCR in the regime dominated by e-e interactions. This interpretation accounts for the bad metallicity and the failed insulator behaviors.

The Mott-like localization can also account for the observed enhanced SN, as follows. Localization results in a metallic state where both the hole localization and hopping are determined by interaction with other holes. Consequently, bunching effects reminiscent of charge blockage due to the localized charge trapping may be expected. In contrast to single-charge trapping on defects manifested by a large and asymmetric bias dependence due to the single-particle energy conservation [57], interaction-driven hopping involves energy transfer among single-particle states explaining the lack of such features for β-Ta. In contrast to blockage by a slowly fluctuating environment, the proposed mechanism involves interaction between tunneling charges themselves, which is expected to result in a white rather than Lorentzian noise spectrum.

Next, we show that the proposed picture explains our tentative observation of Fano factor clustering around even multiples of the FL values, as well as the observed competition between bad metallicity and ferromagnetism. The latter observation suggests spin-dependent pairing incompatible with magnetism. The kinetic energy of holes quasilocalized on the neighboring sites is reduced by maximizing virtual hopping, which for a single orbital results in Mott singlet valence bond (VB) correlations analogous to Cooper pairs, but mediated instead by Coulomb interactions and the Pauli principle. This scenario is not directly applicable to the multiorbital $J = 3/2$ quadruplet. However, the low-symmetry crystal field splits the quadruplet into two Kramers pairs and reduces SOC spin mixing due to the hybridization with the $J = 5/2$ states. Consequently, single orbital-like pseudospin SOC VB correlations due to Mott-Hund interactions are expected (see SM [35] for details), explaining the observed competition with ferromagnetism. A similar mechanism was proposed for $SrIrO_3$, which also exhibits negative TCR at cryogenic T [33].

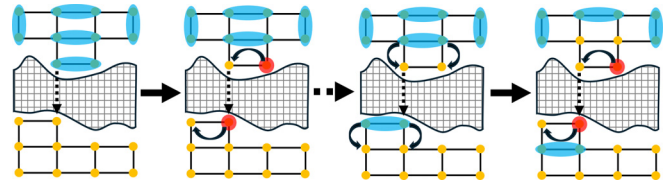

FIG. 5. Correlated tunneling of holes through a hot spot. The blue ovals are VB-like paired states, and the red circles are unpaired holes. The dashed arrows indicate tunneling, and curved arrows indicate hopping in the electrodes.

Because of the structural complexity and multiorbital effects, quantitative analysis of tunneling involving many-electron states in β-Ta is beyond the capabilities of modern computational techniques and will not be attempted here. Qualitatively, we argue that VB-like correlations favor bunched tunneling of even-numbered groups of holes, via a mechanism analogous to charge blockade by localized states in the tunnel barrier but involving quasilocalized holes at the interface. In contrast to Bloch states, tunneling of quasilocalized particles is likely dominated by atomic-scale hot spots. If a hole tunnels out of such a hot spot, the neighboring hole paired to this site by a VB (and which has a large amplitude on this site) is in a higher-energy state due to the lost correlation energy, resulting in an increased probability of its tunneling, as illustrated in Fig. 5. As both holes tunnel, other holes are attracted into the hot spot by Coulomb effects leading to a cascade of tunneling. This proposed effect is similar to trapped charge-induced blockage, where the first tunneling pair plays the role of the trapped charge blocking the tunneling of other hole pairs.

In the proposed picture, device-to-device variability of noise is expected due to the same mechanism as in bunching due to charge trapping in the tunnel barrier [57,58]. Specifically, since tunneling is likely dominated by hot spots, the characteristic number of bunched quasilocalized holes is determined by the local atomic structure of the hot spot, which is expected to vary among different junctions. However, pairing is a robust two-site effect, resulting in clustering around different even values of F.

Because of the competition between disorder and correlations, dynamical disorder should result in reduced bunching, consistent with decreasing F when T is increased (Fig. 2). We attribute the reduction of the Fano factor in TJs with increased bias to a similar mechanism of interaction of localized holes with bias-driven hopping of other holes through the same sites (see SM [35] for details). These mechanisms should be strongly dependent on the atomic environment, which is expected to be manifested by large local variations in measurements by scanning SN microscopy [66].

V. SUMMARY

We presented evidence for a correlated state of quasilocalized electrons manifested by anomalous SN in junctions of a disordered bad metal β-Ta. Bad metals include a variety of

functional materials, among them superconductors with low kinetic inductance and relatively high T_c desirable for photon detectors and quantum information science applications [67–70]. Importantly, the symmetry of VB-like singlets due to Mott-Hund interactions identified in our analysis is the same as that of phonon-mediated Cooper pairs. Thus, superconductivity can be enhanced in these materials by unconventional contributions [71], warranting further studies of correlations in the non-SC state.

Our results have significant implications for spin orbitronics. Contrary to the common interpretations of SHE in β-Ta in terms of its band structure, the single-particle band picture is not applicable to the correlated quasilocalized holes. Remarkably, α-Ta, which is a normal FL, exhibits almost negligible SHE. The relation between bad metallicity and spin-orbitronic efficiency is supported by a giant (order of magnitude) enhancement of SHE in Pt alloys approaching the Ioffe-Regel limit [72,73]. Our analysis indicates that small crystal field effects experienced by quasilocalized electrons enable unquenched atomic orbital moments and consequently a large orbital Hall effect, and thus SHE. The effects of electron correlations on SHE can facilitate efficient correlated orbitronic and spin-orbitronic materials.

ACKNOWLEDGMENTS

We thank Connie Roth and James Merrill for assistance with spectroscopic ellipsometry. Experiments (Y.Z. and S.U.) were supported by NSF Grant No. ECCS-2448290 and in part by the SEED award from the Research Corporation for Science Advancement. Simulations (C.X. and Y.W.) were supported by U.S. Department of Energy (DOE) Office of Science Basic Energy Sciences Early Career Grant No. DE-SC0024524. The simulations used resources of the National Energy Research Scientific Computing Center, a U.S. DOE Office of Science User Facility at Lawrence Berkeley National Laboratory operated under Contract No. DE-AC02-05CH11231.

DATA AVAILABILITY

The data that support the findings of this article are openly available [74]; embargo periods may apply.

[1] J. G. Bednorz and K. A. Müller, Perovskite-type oxides—The new approach to high-T_c superconductivity, Rev. Mod. Phys. **60**, 585 (1988).

[2] N. E. Hussey, II, K. Takenaka, and H. Takagi, Universality of the Mott-Ioffe-Regel limit in metals, Philos. Mag. **84**, 2847 (2004).

[3] T. Zeng, A. Hegg, L. Zou, S. Jiang, and W. Ku, Transport in the emergent Bose liquid: Bad metal, strange metal, and weak insulator, all in one system, arXiv:2112.05747.

[4] X. Zhang, A. Palevski, and A. Kapitulnik, Anomalous metals: From "failed superconductor" to "failed insulator," Proc. Natl. Acad. Sci. USA **119**, e2202496119 (2022).

[5] S. Ono, Y. Ando, T. Murayama, F. F. Balakirev, J. B. Betts, and G. S. Boebinger, Metal-to-insulator crossover in the low-temperature normal state of $Bi_2Sr_{2-x}La_xCuO_{6+\delta}$, Phys. Rev. Lett. **85**, 638 (2000).

[6] Y. Ando, G. S. Boebinger, A. Passner, T. Kimura, and K. Kishio, Logarithmic divergence of both in-plane and out-of-plane normal-state resistivities of superconducting $La_{2-x}Sr_xCuO_4$ in the zero-temperature limit, Phys. Rev. Lett. **75**, 4662 (1995).

[7] S. C. Riggs, J. B. Kemper, Y. Jo, Z. Stegen, L. Balicas, G. S. Boebinger, F. F. Balakirev, A. Migliori, H. Chen, R. H. Liu, and X. H. Chen, Magnetic-field-induced log-T insulating behavior in the resistivity of fluorine-doped $SmFeAsO_{1-x}F_x$, Phys. Rev. B **79**, 212510 (2009).

[8] S. Sahoo, U. Dutta, L. Harnagea, A. K. Sood, and S. Karmakar, Pressure-induced suppression of charge density wave and emergence of superconductivity in $1T-VSe_2$, Phys. Rev. B **101**, 014514 (2020).

[9] H. Lin, J. Si, X. Zhu, K. Cai, H. Li, L. Kong, X. Yu, and H.-H. Wen, Structure and physical properties of $CsV_2Se_{2-x}O$ and V_2Se_2O, Phys. Rev. B **98**, 075132 (2018).

[10] Y. Cao, D. Chowdhury, D. Rodan-Legrain, O. Rubies-Bigorda, K. Watanabe, T. Taniguchi, T. Senthil, and P. Jarillo-Herrero, Strange metal in magic-angle graphene with near Planckian dissipation, Phys. Rev. Lett. **124**, 076801 (2020).

[11] Q. Li, C. He, J. Si, X. Zhu, Y. Zhang, and H.-H. Wen, Absence of superconductivity in bulk $Nd_{1-x}Sr_xNiO_2$, Commun. Mater. **1**, 16 (2020).

[12] L. Zhang, B. Pang, Y. Chen, and Y. Chen, Review of spin-orbit coupled semimetal $SrIrO_3$ in thin film form, Crit. Rev. Solid State Mater. Sci. **43**, 367 (2018).

[13] A. Hegg, J. Hou, and W. Ku, Geometric frustration produces long-sought Bose metal phase of quantum matter, Proc. Natl. Acad. Sci. USA **118**, e2100545118 (2021).

[14] D. Chowdhury, A. Georges, O. Parcollet, and S. Sachdev, Sachdev-Ye-Kitaev models and beyond: Window into non-Fermi liquids, Rev. Mod. Phys. **94**, 035004 (2022).

[15] H. Kim, S. Jamali, and A. Rogachev, Superconductor-insulator transition in long MoGe nanowires, Phys. Rev. Lett. **109**, 027002 (2012).

[16] Y. Qin, C. L. Vicente, and J. Yoon, Magnetically induced metallic phase in superconducting tantalum films, Phys. Rev. B **73**, 100505(R) (2006).

[17] N. P. Breznay and A. Kapitulnik, Particle-hole symmetry reveals failed superconductivity in the metallic phase of two-dimensional superconducting films, Sci. Adv. **3**, e1700612 (2017).

[18] N. P. Breznay, M. Tendulkar, L. Zhang, S.-C. Lee, and A. Kapitulnik, Superconductor to weak-insulator transitions in disordered tantalum nitride films, Phys. Rev. B **96**, 134522 (2017).

[19] C. Christiansen, L. M. Hernandez, and A. M. Goldman, Evidence of collective charge behavior in the insulating state of ultrathin films of superconducting metals, Phys. Rev. Lett. **88**, 037004 (2002).

[20] P. Phillips and D. Dalidovich, The elusive Bose metal, Science **302**, 243 (2003).

[21] Y. Dubi, Y. Meir, and Y. Avishai, Nature of the superconductor-insulator transition in disordered superconductors, Nature (London) **449**, 876 (2007).

[22] P. W. Phillips, Free at last: Bose metal uncaged, Science **366**, 1450 (2019).

[23] C. Yang, Y. Liu, Y. Wang, L. Feng, Q. He, J. Sun, Y. Tang, C. Wu, J. Xiong, W. Zhang, X. Lin, H. Yao, H. Liu, G. Fernandes, J. Xu, J. M. Valles, J. Wang, and Y. Li, Intermediate bosonic metallic state in the superconductor-insulator transition, Science **366**, 1505 (2019).

[24] V. M. Galitski, G. Refael, M. P. A. Fisher, and T. Senthil, Vortices and quasiparticles near the superconductor-insulator transition in thin films, Phys. Rev. Lett. **95**, 077002 (2005).

[25] L. Liu, C.-F. Pai, Y. Li, H. Tseng, D. Ralph, and R. Buhrman, Spin-torque switching with the giant spin Hall effect of tantalum, Science **336**, 555 (2012).

[26] M. Szurek, H. Cheng, Z. Pang, Y. Zhang, J. Bacsa, and S. Urazhdin, Anomalous shot noise in a bad metal β-tantalum, Appl. Phys. Lett. **126**, 082410 (2025).

[27] M. Szurek, H. Cheng, Z. Pang, Y. Zhang, S. Urazhdin, The role of electron interactions revealed by shot noise in a failed insulator, arXiv:2507.05481.

[28] Y. Blanter and M. Büttiker, Shot noise in mesoscopic conductors, Phys. Rep. **336**, 1 (2000).

[29] P. Zhou, L. Chen, Y. Liu, I. Sochnikov, A. T. Bollinger, M.-G. Han, Y. Zhu, X. He, I. Bozovic, and D. Natelson, Electron pairing in the pseudogap state revealed by shot noise in copper oxide junctions, Nature (London) **572**, 493 (2019).

[30] K. M. Bastiaans, D. Chatzopoulos, J.-F. Ge, D. Cho, W. O. Tromp, J. M. van Ruitenbeek, M. H. Fischer, P. J. de Visser, D. J. Thoen, E. F. C. Driessen, T. M. Klapwijk, and M. P. Allan, Direct evidence for Cooper pairing without a spectral gap in a disordered superconductor above T_c, Science **374**, 608 (2021).

[31] A. H. Steinbach, J. M. Martinis, and M. H. Devoret, Observation of hot-electron shot noise in a metallic resistor, Phys. Rev. Lett. **76**, 3806 (1996).

[32] L. Chen, D. T. Lowder, E. Bakali, A. M. Andrews, W. Schrenk, M. Waas, R. Svagera, G. Eguchi, L. Prochaska, Y. Wang, C. Setty, S. Sur, Q. Si, S. Paschen, and D. Natelson, Shot noise in a strange metal, Science **382**, 907 (2023).

[33] Y. Zhang, S. Pandey, S. Ivanov, J. Liu, and S. Urazhdin, Shot noise in a metal close to the Mott transition, Nano Lett. **24**, 15943 (2024).

[34] M. H. Read and C. Altman, A new structure in tantalum thin films, Appl. Phys. Lett. **7**, 51 (1965).

[35] See Supplemental Material at https://link.aps.org/supplemental/10.1103/spvt-n2hz for additional details on measurements, analysis of noise, and mechanisms of bad metallicity and electron pairing, which includes Ref. [36].

[36] W. H. Zurek, Decoherence, einselection, and the quantum origins of the classical, Rev. Mod. Phys. **75**, 715 (2003).

[37] L. W. Nordheim, The effect of the image force on the emission and reflexion of electrons by metals, Proc. R. Soc. A **121**, 626 (1928).

[38] J. G. Simmons, Generalized formula for the electric tunnel effect between similar electrodes separated by a thin insulating film, J. Appl. Phys. **34**, 1793 (1963).

[39] F.-C. Chiu, W.-C. Shih, and J.-J. Feng, Conduction mechanism of resistive switching films in mgo memory devices, J. Appl. Phys. **111**, 094104 (2012).

[40] A. Van Der Ziel, On the noise spectra of semi-conductor noise and of flicker effect, Physica **16**, 359 (1950).

[41] C. W. J. Beenakker and M. Büttiker, Suppression of shot noise in metallic diffusive conductors, Phys. Rev. B **46**, 1889 (1992).

[42] K. E. Nagaev, On the shot noise in dirty metal contacts, Phys. Lett. A **169**, 103 (1992).

[43] K. E. Nagaev, Influence of electron-electron scattering on shot noise in diffusive contacts, Phys. Rev. B **52**, 4740 (1995).

[44] F. Lefloch, C. Hoffmann, M. Sanquer, and D. Quirion, Doubled full shot noise in quantum coherent superconductor-semiconductor junctions, Phys. Rev. Lett. **90**, 067002 (2003).

[45] J. I. Budnick, Some studies of the superconducting transition in purified tantalum, Phys. Rev. **119**, 1578 (1960).

[46] T. Jabegu, N. Li, A. Okmi, B. Tipton, I. Vlassiouk, K. Xiao, S. Urazhdin, Y. Yao, and S. Lei, Interfacial momentum matching for Ohmic van der Waals contact construction, Adv. Electron. Mater. **11**, 2400397 (2024).

[47] J. W. Furness, A. D. Kaplan, J. Ning, J. P. Perdew, and J. Sun, Accurate and numerically efficient r^{2}SCAN meta-generalized gradient approximation, J. Phys. Chem. Lett. **11**, 8208 (2020).

[48] W. Huang, D.-H. Xing, J.-B. Lu, B. Long, W. H. E. Schwarz, and J. Li, How much can density functional approximations (DFA) fail? The extreme case of the FeO_4 species, J. Chem. Theory Comput. **12**, 1525 (2016).

[49] R. Kingsbury, A. S. Gupta, C. J. Bartel, J. M. Munro, S. Dwaraknath, M. Horton, and K. A. Persson, Performance comparison of r^2SCAN and SCAN metaGGA density functionals for solid materials via an automated, high-throughput computational workflow, Phys. Rev. Mater. **6**, 013801 (2022).

[50] P. Giannozzi, O. Andreussi, T. Brumme, O. Bunau, M. B. Nardelli, M. Calandra, R. Car, C. Cavazzoni, D. Ceresoli, M. Cococcioni, *et al.*, Advanced capabilities for materials modelling with QUANTUM ESPRESSO, J. Phys.: Condens. Matter **29**, 465901 (2017).

[51] J. P. Perdew, K. Burke, and M. Ernzerhof, Generalized gradient approximation made simple, Phys. Rev. Lett. **77**, 3865 (1996).

[52] D. R. Hamann, Optimized norm-conserving Vanderbilt pseudopotentials, Phys. Rev. B **88**, 085117 (2013).

[53] S. Grimme, Semiempirical GGA-type density functional constructed with a long-range dispersion correction, J. Comput. Chem. **27**, 1787 (2006).

[54] H. J. Monkhorst and J. D. Pack, Special points for Brillouin-zone integrations, Phys. Rev. B **13**, 5188 (1976).

[55] E. V. Bezuglyi, E. N. Bratus', V. S. Shumeiko, and G. Wendin, Multiple andreev reflections and enhanced shot noise in diffusive superconducting-normal-superconductor junctions, Phys. Rev. Lett. **83**, 2050 (1999).

[56] S. S. Safonov, A. K. Savchenko, D. A. Bagrets, O. N. Jouravlev, Y. V. Nazarov, E. H. Linfield, and D. A. Ritchie, Enhanced shot noise in resonant tunneling via interacting localized states, Phys. Rev. Lett. **91**, 136801 (2003).

[57] S. Garzon, Y. Chen, and R. Webb, Enhanced spin-dependent shot noise in magnetic tunnel barriers, Physica E **40**, 133 (2007).

[58] Y. Zhang and G. Xiao, Spin-dependent shot noise in MgO-based magnetic tunnel junctions under noncollinear magnetization alignment, Phys. Rev. B **100**, 224402 (2019).

[59] M. Magnuson, G. Greczynski, F. Eriksson, L. Hultman, and H. Högberg, Electronic structure of β-Ta films from x-ray photoelectron spectroscopy and first-principles calculations, Appl. Surf. Sci. **470**, 607 (2019).

[60] A. Jiang, A. Yohannan, N. O. Nnolim, T. A. Tyson, L. Axe, S. L. Lee, and P. Cote, Investigation of the structure of β-tantalum, Thin Solid Films **437**, 116 (2003).

[61] O. K. Andersen, W. Klose, and H. Nohl, Electronic structure of Chevrel-phase high-critical-field superconductors, Phys. Rev. B **17**, 1209 (1978).

[62] J. Jenke, A. N. Ladines, T. Hammerschmidt, D. G. Pettifor, and R. Drautz, Tight-binding bond parameters for dimers across the periodic table from density-functional theory, Phys. Rev. Mater. **5**, 023801 (2021).

[63] J. C. Slater and G. F. Koster, Simplified LCAO method for the periodic potential problem, Phys. Rev. **94**, 1498 (1954).

[64] J. Lee, K.-H. Jin, A. Catuneanu, A. Go, J. Jung, C. Won, S.-W. Cheong, J. Kim, F. Liu, H.-Y. Kee, and H. W. Yeom, Honeycomb-lattice Mott insulator on tantalum disulphide, Phys. Rev. Lett. **125**, 096403 (2020).

[65] L. de' Medici, Hund's coupling and its key role in tuning multiorbital correlations, Phys. Rev. B **83**, 205112 (2011).

[66] K. M. Bastiaans, D. Cho, D. Chatzopoulos, M. Leeuwenhoek, C. Koks, and M. P. Allan, Imaging doubled shot noise in a Josephson scanning tunneling microscope, Phys. Rev. B **100**, 104506 (2019).

[67] M. S. Osofsky, R. J. Soulen, J. H. Claassen, G. Trotter, H. Kim, and J. S. Horwitz, New insight into enhanced superconductivity in metals near the metal-insulator transition, Phys. Rev. Lett. **87**, 197004 (2001).

[68] K. Wakasugi, M. Tokunaga, T. Sumita, H. Kubota, M. Nagata, and Y. Honda, Superconductivity of reactivity sputtered TaN film for ULSI process, Physica B **239**, 29 (1997).

[69] S. Mandal, S. Dutta, S. Basistha, I. Roy, J. Jesudasan, V. Bagwe, L. Benfatto, A. Thamizhavel, and P. Raychaudhuri, Destruction of superconductivity through phase fluctuations in ultrathin a-MoGe films, Phys. Rev. B **102**, 060501(R) (2020).

[70] P. Chauhan, R. Budhani, and N. P. Armitage, Anomalously small superconducting gap in a strong spin-orbit coupled superconductor: β-tungsten, Phys. Rev. B **105**, L060503 (2022).

[71] Y.-J. Zhang, Y. Zhu, Q. Li, Z.-N. Xiang, T. Huang, J. Sun, and H.-H. Wen, Record-high superconducting transition temperature in a $Ti_{1-x}Mn_x$ alloy with the rich magnetic element Mn, J. Am. Chem. Soc. **146**, 21110 (2024).

[72] U. Shashank, T. Tomoda, A. J. Mathew, G. Vashisht, K. Imai, Y. Kusaba, C.-L. Dong, C.-L. Chen, Y. Horibe, M. Ishimaru, H. Awano, H. Asada, and Y. Fukuma, Giant spin-orbit torque induced by spin Hall effect in amorphous Pt(P) alloys, NPG Asia Mater. **17**, 15 (2025).

[73] Q. Liu and L. Zhu, Enhancing z spin generation in trivial spin Hall materials for scalable, energy-efficient, field-free, complete spin-orbit torque switching applications, Adv. Sci. **12**, e07581 (2025).

[74] S. Urazhdin, Data and figures for the manuscript "Evidence for correlated electron state from shot noise in "bad" metal nanojunctions", Zenodo (2025), http://doi.org/10.5281/zenodo.17268050.